Novel Cooperative Interactions and Structural Ordering in H_2S-H_2

Timothy A. Strobel,[1,*] P. Ganesh,[2,†] Maddury Somayazulu,[1] P. R. C. Kent,[2] and Russell J. Hemley[1]
[1]Geophysical Laboratory, Carnegie Institution of Washington, Washington, D.C. 20015, USA
[2]Center for Nanophase Materials Sciences, Oak Ridge National Laboratory, Oak Ridge, Tennessee 37831, USA
(Received 5 July 2011; published 16 December 2011)

Hydrogen sulfide (H_2S) and hydrogen (H_2) crystallize into a 'guest-host' structure at 3.5 GPa and, at the initial formation pressure, the rotationally disordered component molecules exhibit weak van der Waals-type interactions. With increasing pressure, hydrogen bonding develops and strengthens between neighboring H_2S molecules, reflected in a pronounced drop in S-H vibrational stretching frequency and also observed in first-principles calculations. At 17 GPa, an ordering process occurs where H_2S molecules orient themselves to maximize hydrogen bonding and H_2 molecules simultaneously occupy a chemically distinct lattice site. Intermolecular forces in the $H_2S + H_2$ system may be tuned with pressure from the weak hydrogen-bonding limit to the ordered hydrogen-bonding regime, resulting in a novel clathrate structure stabilized by cooperative interactions.

DOI: 10.1103/PhysRevLett.107.255503 PACS numbers: 81.40.Vw, 61.66.Fn, 62.50.−p, 82.30.Rs

At high density, mixtures of nonpolar molecules may form stoichiometric compounds stabilized by weak van der Waals forces [1–3], while hydrogen-bonding molecules like H_2O form clathrate compounds stabilized by cooperative guest-host interactions [4]. An accurate description of intermolecular interactions between these types of simple molecules is required to describe a variety of phenomena relevant to chemical and condensed matter physics. In contrast with H_2O, H_2S exhibits little to no hydrogen bonding at ambient pressure. While valence isoelectronic and geometrically congruous with H_2O, H_2S undergoes a series of pressure-induced phase transitions that are structurally incompatible with those observed for water [5]. Between 0.5 and 11 GPa, H_2S goes through three phase transitions, shifting from a rotationally disordered solid to an ordered H-bonded structure [6–9]. Variation in hydrogen-bond strength with pressure dictates structural transformations for the pure component [9], yet it is unclear how H_2S structural motifs would vary in high-pressure mixtures. The ability of pressure to tune hydrogen-bonding strength, from absent to structurally important, provides an opportunity to explore compound formation in the weak hydrogen-bonding limit, and to clarify how intermolecular interactions may change over a range of densities. Here we present the formation of a novel compound comprised of H_2S and H_2. This compound initially behaves as a weakly interacting van der Waals solid, eventually ordering into a hydrogen-bonded clathrate structure through application of external pressure.

Mixtures of H_2S and H_2 were loaded into diamond anvil cells by a combination of cryogenic and gas loading methods [10]. Samples loaded near 0.2 GPa exhibited two equilibrium phases at room temperature (liquid H_2S and fluid H_2) with limited mutual solubility. At ~1 GPa, H_2S solidified, completely excluding previously dissolved H_2. Raman spectra obtained from the solid H_2S phase are consistent with reports for phase I [11]. Fluid hydrogen and solid phase I of H_2S coexisted until ~3.5 GPa where a new solid nucleated and crystals of columnar habit began growing into the H_2 fluid phase (Fig. 1).

At 4.5 GPa, synchrotron x-ray diffraction (XRD) patterns obtained from the compound were readily indexed to a tetragonal lattice with $a = 7.37(3)$ Å and $c = 6.07(2)$ Å,

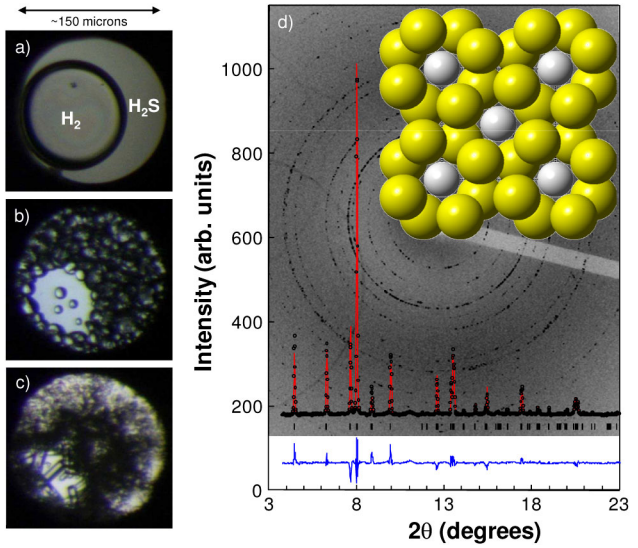

FIG. 1 (color online). Photomicrographs of $H_2 + H_2S$ mixtures at room temperature: (a) 0.2 GPa: fluid H_2 and liquid H_2S; (b) 1.0 GPa: fluid H_2 and solid H_2S phase I; (c) 3.5 GPa: fluid H_2 and compound. Dark areas result from light scattering off grain boundaries and dissipated with time. (d) Experimental diffraction pattern ($\lambda = 0.40548$ Å) at 4.5 GPa (points) and Rietveld profile refinement (red line). Difference is shown as lower blue trace, $R_{wp} = 3.52\%$. The background shows the two-dimensional diffraction image, and the crystal structure, normal to the c-axis, is provided as the inset: yellow and white spheres represent disordered H_2S and H_2 molecules, respectively.

and systematic absences constrained the space-group to $I4/mcm$. A survey of tetragonal crystal structures with similar c/a ratios suggested the compound was of the Al_2Cu type [12]. Rietveld profile refinement assuming this structural model produced excellent agreement with experimental data using sulfur atoms at the 8h Wyckoff positions ($x = 0.162$). The compound stoichiometry $(H_2S)_2H_2$, with 4 f.u. per cell, was thus inferred from the structure type, where hydrogen molecules are centered at the 4a sites. This composition is further supported by the volume obtained by the assemblage of pure component species (0.7% difference at 4.5 GPa)[7,8,13].

The Al_2Cu structure may be viewed as a guest-host type arrangement where hydrogen molecules are hosted within channels formed by a framework comprised of alternating H_2S layers along the c axis. This assembly is similar to the complex guest-host structures observed in alkali and alkaline earth metals at high pressure as well as other intermetallic compounds [14]. Thus, the formation of the alloy-type $(H_2S)_2H_2$ compound is likely dictated by efficient molecular packing rather than significant hydrogen bonding. Indeed, the same structure type was observed for $CH_4 + H_2$ at high pressure [3]; the diameter of CH_4 (~ 3.8 Å) is comparable to that of H_2S (~ 3.6 Å).

At the formation pressure, contributions to the Raman spectrum from H_2S are similar to the phase I solid [11], indicating rotational disorder of component molecules. The symmetric and antisymmetric ν_1 and ν_3 stretching modes are convoluted into a broad band shifted to higher frequency by 10 cm^{-1} when compared with the pure solid (Fig. 2). A broad density-of-states-like feature appears in the low-frequency region which contains hydrogen rotational contributions. The H_2 vibron originating from the compound is shifted to lower frequency by 30 cm^{-1} compared with the bulk fluid, and the presence of a single contribution is consistent with H_2 occupation of a single lattice site and the Al_2Cu type crystal structure. The S-H stretching frequency decreased monotonically with pressure, indicating a progressive strengthening of hydrogen bonding, analogous to bulk solid H_2S.

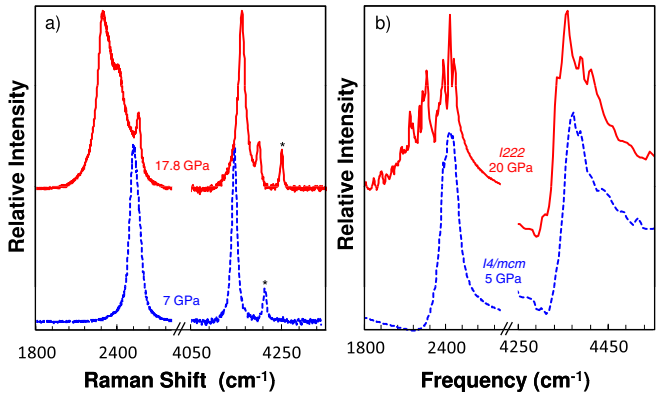

FIG. 2 (color online). (a) Experimental Raman spectra obtained from the $H_2 + H_2S$ compound with pressure. Bulk H_2 vibron denoted by asterisk. (b) Calculated VDOS in S-H and H-H stretching regions at 150 K for $I4/mcm$ and $I222$ structures with Gaussian smearing of 5 cm^{-1}.

At 17 GPa, a distinct ordering process occurs as evidenced by drastic changes in the Raman spectra (Fig. 2). The S-H stretching region splits into several contributions, similar to, yet distinct from phase IV of pure H_2S [15]. The change from a broad and unstructured spectrum to one of a multiplet nature suggests a transition from free rotation to ordered hydrogen bonds, akin to the bulk phase I' to IV transition. In addition, multiple low-frequency lattice modes appear above 17 GPa, consistent with the constraining of free rotation to translation or libration. The hydrogen vibron splits from a single broad band into two discrete contributions. The two components are separated by nearly 40 cm^{-1}, the most perturbed of which is $\sim$90 cm^{-1} softer than bulk H_2 at 17 GPa.

While the Raman observations support a structural phase transformation at 17 GPa, synchrotron XRD patterns obtained over this pressure range showed no clear indication of a structural change [Fig. 3(a)]. All patterns measured at these pressures could be indexed to the

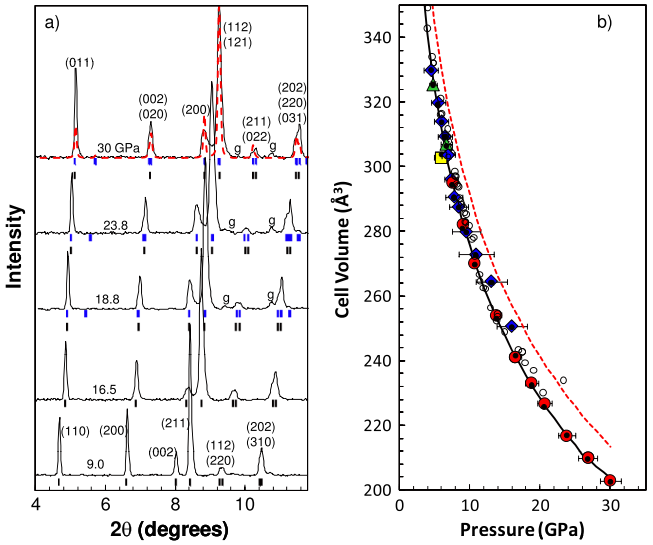

FIG. 3 (color online). (a) Synchrotron XRD patterns with pressure ($\lambda = 0.39796$ Å). At 18.8 GPa and above, tick marks indicate reflections for $I4/mcm$ (lower ticks) and $I222$ (upper ticks) ; Miller indices are labeled for the two structures in the bottom and top patterns, respectively. Gasket contributions are labeled 'g'. A simulated XRD pattern based on the calculated $I222$ structure at 30 GPa (dashed). The powder quality of this sample was poor; Bragg intensity varied significantly depending on x-ray position. (b) Equation of state. Large filled symbols are experimental data from independent runs. Error bars give the maximum pressure gradient across the cell from multiple ruby pieces. Small open symbols show pure component volumes: $4(2H_2S + H_2)$. Small filled circles show the volume obtained from $I222$ indexing. The solid black and dashed red lines are the calculated EOS for the $I222$ and $I4/mcm$ structures, respectively.

$I4/mcm$ structure, and no obvious discontinuity was observed in the equation of state (EOS). The diffraction data provide no clear support for alternative indexing, suggesting that the sulfur atomic positions remain largely unchanged and that the transition is associated with displacements in atomic hydrogen positions.

In order to further elucidate the nature of the spectroscopically observed transition at 17 GPa, *ab initio* density functional theory (DFT) calculations were performed as implemented in VASP [16–19]. Starting from the experimental $I4/mcm$ structure at 5 GPa, the EOS for the optimized structure was calculated using fully symmetry-constrained relaxation of the atomic positions and lattice strain with stresses converged to 0.01 kB [Fig. 3(b)] [19]. The resulting EOS showed reasonable agreement compared to experimental data with a +5.6% average deviation over the entire pressure interval.

Because the experimental Raman data indicate structural changes above 17 GPa, yet XRD data show little difference, variants of the $I4/mcm$ structure were obtained by distributing H_2 occupancy across the f or g sites and/or changing orientations of H_2S molecules [19]. Several permutations were optimized over a range of pressures, resulting in the prediction of a new stable high-pressure structure of symmetry $I222$. The $I222$ phase is related to $I4/mcm$ by a subgroup reduction in symmetry, yielding two unique H_2 sites and an ordered, H-bonded H_2S lattice. This structure consists of H-bonded H_2S zigzag sheets that trap hydrogen molecules in channels along the a axis [Figs. 4(a) and 4(b)]. This arrangement is comparable to the guest-host clathrate structures found in urea [20]. Strong hydrogen bonds are formed along the H_2S chains that roughly follow the a axis (S-H $\cdots$ S = 1.8 Å) whereas weaker ones are formed along the chains that follow the b axis (S-H $\cdots$ S = 2.27 Å). The strong hydrogen bonding significantly elongates the H_2S covalent bond, producing two unique S-H distances for a single molecule: 1.45 and 1.35 Å for the quasi-a and -b directions, respectively. This anisotropy is similar to that found in ice II, where stronger inter-ring hydrogen bonding produces elongated O-H covalent distances relative to those observed between ring layers [21]. A distribution of S-H distances is supported experimentally by the large range observed for S-H stretching frequencies.

The calculated EOS for $I222$ produced excellent agreement with experimental data showing an average −0.2% deviation over the entire pressure range [Fig. 3(b)]. $I222$ is enthalpically stablilized relative to $I4/mcm$ at all pressures; however, this stability increases steeply from 40 meV/atom at 4 GPa to 115 meV/atom at 30 GPa. An ordered $I222$ ground state is similar to low-pressure experimental observations; at 1.5 K and atmospheric pressure, pure H_2S takes on an ordered orthorhombic structure [6].

Based on theoretical predictions of the low-enthalpy $I222$ structure, experimental diffraction patterns were analyzed considering this phase. At low pressure, all XRD patterns were described well by the $I222$ structure, however, Rietveld refinements assuming $I222$ showed slightly poorer fits than $I4/mcm$ ($R_{wp} = 3.80\%$ vs $R_{wp} = 3.52\%$), and refined orthorhombic distortions were insignificant: $a/b = 0.8232(2)$ and $a/c = 0.8233(2)$. These distortions are compared with the DFT values of $a/b = 0.804$ and $a/c = 0.756$ at 5 GPa. For $I4/mcm$, the calculated $c/a = 0.826$ agrees well with the experimental value of 0.8233(2). The excellent agreement between experimental and calculated $I222$ volumes at low pressure is a consequence of an under-prediction in the a and b cell lengths compensated by an over-prediction in c. At 19 GPa, agreement between calculated ($a/b = 0.820$ and $a/c = 0.788$) and experimental ($a/b = 0.832(1)$ and $a/c = 0.822(1)$) lattices was much better. Although the presence of coarse-grained crystals in the high-pressure sample precluded detailed Rietveld refinements, simulated XRD patterns based on the $I222$ structure showed very reasonable agreement with experiment [Fig. 3(a)]. Based on the EOS and the structural refinement comparison with calculations, we suggest that the symmetry of the low-pressure phase is $I4/mcm$ while the high-pressure phase is $I222$. We note that in the absence of experimental knowledge for H-atom positions, the absolute symmetry of the low-pressure phase might be lower than $I4/mcm$; however, this lattice is

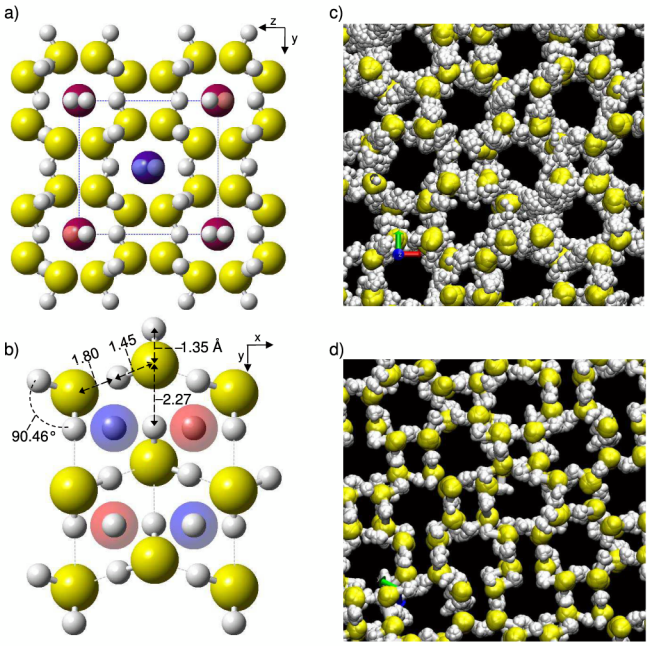

FIG. 4 (color online). (a) $I222$ structure normal to the (100) plane. (b) Hydrogen-bonding motif normal to the (001) plane. Bond distances are labeled, translucent red and blue spheres indicate different H_2 sites. Overlapping configurations from AIMD trajectories showing H-atom (H_2S) density distribution for (c)$I4/mcm$ at 5 GPa and (d) $I222$ at 20 GPa. H_2 molecules are not shown for clarity.

consistent with rotational disorder and other molecular and nonmolecular alloys.

To further investigate dynamics and interactions at finite temperature, *ab initio* molecular dynamics (AIMD) simulations were performed for both the $I4/mcm$ and $I222$ structures using a Nosé-Hoover thermostat at 300, 150, and 77 K [19]. The AIMD simulations revealed a picture of interactions consistent with the spectroscopic data. At 5 GPa, the $I4/mcm$ structure shows nearly free rotation of H_2 and H_2S about molecular centers with the presence of sporadic and short-lived hydrogen-bond contacts [Fig. 4(c)]. As pressure increases from 5 to 30 GPa, increased hydrogen bonding leads to more orientational ordering of H_2S molecules, so H atoms lie between S atoms with greater probability. At 20 GPa, AIMD trajectories reveal ordered hydrogen bonds for the $I222$ structure, showing only small librational motions of H_2S H atoms from equilibrium positions [Fig. 4(d)].

The vibrational density of states (VDOS) was computed from the Fourier-transform of the velocity autocorrelation function using AIMD trajectories at 5 and 20 GPa [19]. The general features of the $I4/mcm$ VDOS agree qualitatively with Raman spectra: a single H_2 vibron feature and S-H stretching band, both of which broaden with pressure (Fig. 2). At 20 GPa, the $I222$ VDOS also agrees qualitatively with experimental spectra, showing a structured S-H stretching region and multiple low-frequency contributions [19]. The $I222$ H_2 stretching region also shows increased splitting over a larger frequency range relative to $I4/mcm$, suggesting the second crystallographic site as the origin for the observed H_2 vibron splitting.

The $H_2S + H_2$ compound is stabilized by cooperative interactions, the nature of which changes under pressure. At low pressure, component molecules interact weakly through dispersional forces. As pressure increases, hydrogen bonding develops between neighboring H_2S molecules until ordering occurs near 17 GPa. This hydrogen bonding, however, is not solely sufficient for stability. When hydrogen molecules are removed from the lattice, AIMD simulations reveal that the H_2S molecules collapse to a largely disordered state. Thus, two primary interactions give rise to stability in this system: attractive hydrogen-bonding between H_2S molecules and repulsion between H_2 and nearest-neighbor H_2S molecules, which restrict H_2S orientations in a manner so as to maximize hydrogen-bonding between them. While pressure was previously correlated with increased hydrogen-bond strength, this role in molecular compounds is now clearer. Pressure tunes intermolecular forces from the weakly-interacting limit into the strongly hydrogen-bonded regime where guest-host clathrate structures are formed.

We thank Y. Meng and O. Shebanova for help with XRD and M. Guthrie and D. A. Dalton for helpful comments. We acknowledge support from DOE-BES (DE-FG02-06ER46280), NSF-DMR (DMR-0805056) and DOE-NNSA (DE-FC52-08NA28554). Portions of this work were performed at HPCAT (Sector 16, APS, ANL). P. R. C. K. was supported by the Center for Nanophase Materials Sciences, which is sponsored at ORNL by DOE-BES. Computations used the NERSC supported by DOE-SC No. DE-AC02-05CH11231.

*tstrobel@ciw.edu
†ganeshp@ornl.gov

[1] W. L. Vos, L. W. Finger, R. J. Hemley, J. Z. Hu, H. K. Mao, and J. A. Schouten, Nature (London) **358**, 46 (1992).
[2] P. Loubeyre, R. Letoullec, and J. P. Pinceaux, Phys. Rev. Lett. **72**, 1360 (1994).
[3] M. S. Somayazulu, L. W. Finger, R. J. Hemley, and H. K. Mao, Science **271**, 1400 (1996).
[4] E. D. Sloan and C. A. Koh, *Clathrate Hydrates of Natural Gases* (Taylor & Francis/CRC Press, Boca Raton, 2008), 3rd ed.
[5] S. Endo, N. Ichimiya, K. Koto, S. Sasaki, and H. Shimizu, Phys. Rev. B **50**, 5865 (1994).
[6] J. K. Cockcroft and A. N. Fitch, Z. Kristallogr. **193**, 1 (1990).
[7] H. Fujihisa, H. Yamawaki, M. Sakashita, K. Aoki, S. Sasaki, and H. Shimizu, Phys. Rev. B **57**, 2651 (1998).
[8] S. Endo, A. Honda, K. Koto, O. Shimomura, T. Kikegawa, and N. Hamaya, Phys. Rev. B **57**, 5699 (1998).
[9] J. S. Loveday, R. J. Nelmes, S. Klotz, J. M. Besson, and G. Hamel, Phys. Rev. Lett. **85**, 1024 (2000).
[10] T. A. Strobel, X. J. Chen, M. Somayazulu, and R. J. Hemley, J. Chem. Phys. **133**, 164512 (2010).
[11] H. Shimizu, Y. Nakamichi, and S. Sasaki, J. Chem. Phys. **95**, 2036 (1991).
[12] A. J. Bradley and P. Jones, J. Inst. Met. **51**, 131 (1933).
[13] R. J. Hemley, H. K. Mao, L. W. Finger, A. P. Jephcoat, R. M. Hazen, and C. S. Zha, Phys. Rev. B **42**, 6458 (1990).
[14] O. Degtyareva, High Press. Res. **30**, 343 (2010).
[15] H. Shimizu, H. Yamaguchi, S. Sasaki, A. Honda, S. Endo, and M. Kobayashi, Phys. Rev. B **51**, 9391 (1995).
[16] G. Kresse and J. Furthmüller, Phys. Rev. B **54**, 11169 (1996).
[17] G. Kresse and D. Joubert, Phys. Rev. B **59**, 1758 (1999).
[18] P. E. Blöchl, Phys. Rev. B **50**, 17953 (1994).
[19] See Supplemental Material at http://link.aps.org/supplemental/10.1103/PhysRevLett.107.255503 for methods and supporting information.
[20] A. E. Smith, Acta Crystallogr. **5**, 224 (1952).
[21] C. Lobban, J. L. Finney, and W. F. Kuhs, J. Chem. Phys. **117**, 3928 (2002).